Study on Capillary Properties of Braided Wire Wick for Heat Pipes

Yohan Kim and Hyungdae Kim*
Department of Nuclear Engineering, Kyung Hee University, Republic of Korea
**Corresponding author: hdkims@khu.ac.kr*

***Keywords: heat pipe, braided wire wick, capillary property**

1. Introduction

A capillary-driven heat pipe is expected to be utilized in a nuclear reactor for space missions as a passive, reliable, and compact heat transfer device with no moving parts. Korea Atomic Energy Research Institute (KAERI) is developing a heat pipe-cooled reactor for lunar surface power. Due to the size difference between the reactor core and heat engine and to maximize utilization in space conditions, a bendable heat pipe is one of the critical aspects of the development [1].

When the heat pipe is bent, the deformation of a wick structure in contact with the inner wall of the tube affects its performance. Previous studies have indicated that traditional wicks, such as grooved, sintered powder, and screen wicks, tend to deform when bent, leading to potential damage or separation from the container wall [2, 3]. Such deformations can significantly reduce the heat transport capabilities of these heat pipes.

In response to this challenge, KAERI has proposed the use of a spring-like braided wire wick structure for bendable heat pipes due to its reliable bending capability and high elasticity [1]. In the design phase of these heat pipes, it is crucial to evaluate their operational performance, including heat transport limits like the capillary and entrainment limits. The operational performance is affected by the flow characteristics within the wick, which are determined by the wick's capillary properties as a porous medium. The capillary properties are porosity, effective capillary radius, and permeability. The effective capillary radius determines the capillary limit, and the porosity and permeability determine pressure drops through the wick structure. Therefore, it is crucial to predict the capillary properties of the wick structure.

Unlike conventional wicks such as grooved, sintered powder, and screen wicks, there is currently no model for predicting the capillary properties of braided wire wicks. Several studies have been conducted on the capillary property models of wicks similar to braided wire wicks. For the permeability, most of them used the models that had been developed for other wick structures like screen mesh wick and sintered wick, such as the Carman-Kozeny model [4-8] or as a similar structure wick the braided wire wick, parallel wire bundles [9]. For the effective capillary radius, some studies used their idealized model to predict [4, 5]. In these studies, there was no direct experimental validation of the models, so it is hard to evaluate the validity of the existing models' predictions for the braided wire wick. Thus, it is necessary to establish and validate a suitable model for the braided wire wick. In response to this need, in this study, the capillary properties of braided wire wicks were investigated theoretically with the suitable existing models and evaluated their validities experimentally.

2. Theoretical analysis

2.1. Structure of the braided wire wick

As general characteristics, the braided wire wick has cylindrical geometry, and strands of metal wires are braided in a spiral way, which has a spring-like structure that makes it highly elastic. A schematic of the wire strand is in Fig. 1.

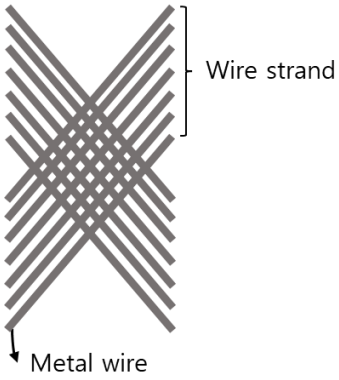

Fig. 1. Schematic of the wire strand and each metal wire of the braided wire wick.

Although the wire diameter of the braided wire wick proposed by KAERI is 0.20 mm [1], a braided wire wick with the same specifications as KAERI's braided wire wick except for the wire diameter, whose value was 0.25 mm, was used for this study because of the manufacturability. Table I and Fig. 1 contain side and cross-sectional views and specifications of the braided wire wick in this study. The thickness of the wick was measured using electrical vernier calipers within 0.01 mm uncertainty.

Table I: Specifications of braided wire wick in this study

Specification	Value
Material	Stainless steel 304
Wire diameter	0.25 mm
Thickness	0.75 mm
Nominal outer diameter	14 mm
Wires per strand	7 wires

Fig. 2. Side and cross-sectional views of the braided wire wick in this study.

2.2. Observation of the capillary flow

Before the theoretical analysis, a preliminary visualization experiment was conducted to observe and understand the capillary phenomenon in the braided wire wick. The wick sample was cleaned and dipped vertically into deionized (DI) water. Then, the capillary flow through the wick was observed using a high-speed camera. A main observation was the capillary flow occurs only between the wires. There was no flow observed in the space with no wires. This seems to be because the capillary force is mainly formed between the wires, which could make the capillary flow against gravity. The raw visualization data and the direction of the flow with its cross-section are depicted in Fig. 3.

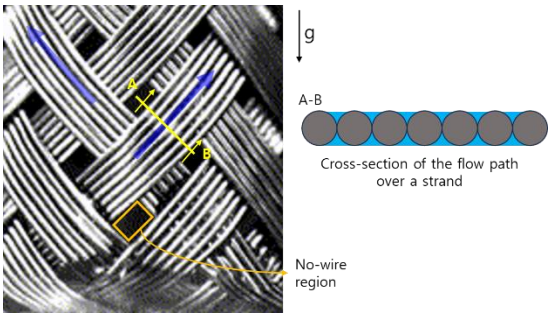

Fig. 3. Raw visualization data of the preliminary experiment and the direction of the capillary flow through the braided wire wick with its cross-section.

2.3. Models for the analysis

Based on a literature survey, several models were established to evaluate the capillary properties of the braided wire wick. Although the liquid will flow through the no-wire regions in the actual situation in the heat pipe, the capillary properties within the main capillary flow paths were evaluated, which was observed in the preliminary experiment.

2.3.1. Geometric model and evaluation of the porosity

As a geometric model for the analysis, the basic geometric model from the former study [10] was simplified using the assumption that all adjacent wires contact with each other (tightly wrapped). Due to the interval between the wires being hard to quantify practically, this assumption made the model more straightforward in analyzing the braided wire wick. The model is based on a unit cell of the braided wire wick, which is a repeated rhombus area that has four middle points of strands' intersections as vertices. Several basic parameters define the model's geometry, and some derived parameters can be obtained using them. Because of the elasticity of the braided wire wick, some of its parameters are changed by the inner diameter of the heat pipe tube where it is inserted, which is identical to the outer diameter of the wick. In the case of the primary parameters, once they are measured in the nominal state of the wick, their values are fixed regardless of the heat pipe tube's diameter. On the other hand, the derived parameters except M are varied with the heat pipe tube's diameter. The intersection angle of strands especially increases as the tube's diameter decreases. The geometry of the liquid flow paths can be analyzed using them. The model and its parameters are depicted in Fig. 4, and the primary and derived parameters are listed in Table II and Table III, respectively, with their values for the braided wire wick.

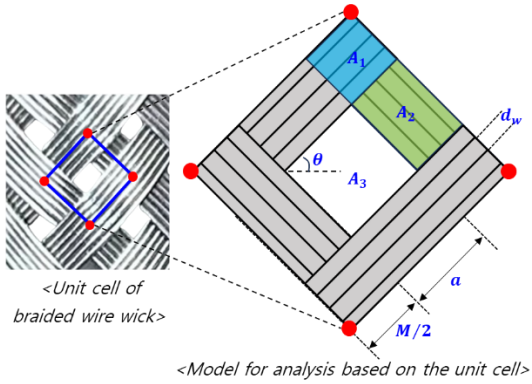

Fig. 4. Geometric model of the braided wire wick based on its unit cell.

Table II: Primary parameters that define the model [10] and the values for the braided wire wick in this study

Parameter	Symbol	Value
Wire diameter	d_w	0.25 mm
Number of wires per strand	m	7 wires
Length of a strand per turn	L_0	62 mm
Nominal outer diameter	D_0	14 mm
Number of strands per turn	n	12 strands

Table III: Derived parameters from the basic parameters

Parameter	Symbol	Value
Width of a strand	M	1.75 mm
Interval between strands	a	0.84 mm
Intersection angle of strands	θ	45°
Area of two overlapped strands	A_1	0.77 mm^2
Area of one strand	A_2	0.74 mm^2
Area of no wires	A_3	0.71 mm^2

The derived parameters were calculated by Eq. 1 to 5, which are relations between the parameters.

(1) $a = \frac{\pi D_0 \sin\theta}{n} - M$

(2) $\cos\theta = \frac{\pi D_0}{L_0}$ & $\sin\theta = \frac{\sqrt{L_0^2 - \pi^2 D_0^2}}{L_0}$

(3) $A_1 = \frac{M^2}{8\sin\theta\cos\theta}$

(4) $A_2 = \frac{aM}{4\sin\theta\cos\theta}$

(5) $A_3 = \frac{a^2}{2\sin\theta\cos\theta}$

The porosity of the braided wire wick was calculated using a geometric analysis of the model. Based on the assumption that the wire strands are piecewise linear, cross-sectional views of each side of the model are in Fig. 5.

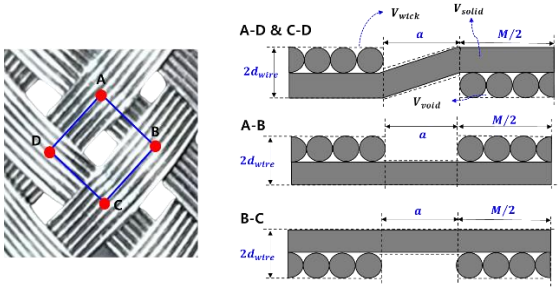

Fig. 5. Cross-sectional views of each side of the geometric model.

Based on the findings from the preliminary experiment, the spaces between the adjacent wires, which were the liquid's flow paths, were considered the wick's void volume, and the region without wires was not considered for the porosity. Then, the porosity of the braided wire wick, ε_B, which is defined as the ratio of the void volume to the wick's total volume, can be calculated according to Eq. 6.

(6) $\varepsilon_B = 1 - \frac{V_{wires}}{V_{wick}} = 1 - \frac{\pi/_2 d_w^2 m(a+M)}{d_w(8A_1+4A_2)} = 1 - \frac{\pi\sin 2\theta}{4}$

V_{wires} is the volume of the wires (solid), and V_{wick} is the volume of the total wick with void. To make the model only with the primary parameter, with Eq. 2, Eq. 6 can be expressed using the outer diameter and length of a strand per its turn along the perimeter of the wick.

(7) $\varepsilon_B = 1 - \frac{\pi^2 D_0\sqrt{L_0^2 - \pi^2 D_0^2}}{2L_0^2}$

With Eq.7, the porosity of the braided wire wick can be calculated using the inner diameter of the heat pipe. In this work, the calculated wick's porosity value was 0.21.

2.3.2. Models for effective capillary radius and permeability

Capillary models of the braided wire wick were established for the capillary flow between the wires, which was observed as the primary source of capillary force. Then, the effective capillary radius and permeability were evaluated using the models.

Effective capillary radius

The effective capillary radius, r_{eff}, is defined as the maximum curvature of a liquid meniscus in the wick structure [11]. Due to the continuous paths of the capillary flow consisting of parallel wires, the model of the wick structure that consists of a series of parallel wires was chosen for the effective capillary radius. According to the model, the effective capillary radius of the parallel wires is wire spacing [11], which is the wire diameter of the braided wire wick based on the geometric model. A schematic of the model is in Fig. 6. Therefore, the theoretical value of the effective capillary radius of the wick, r_{eff_B} in this work is given by Eq. 8.

(8) $r_{eff\_B} = wire\ spacing = d_w = 0.25$ mm

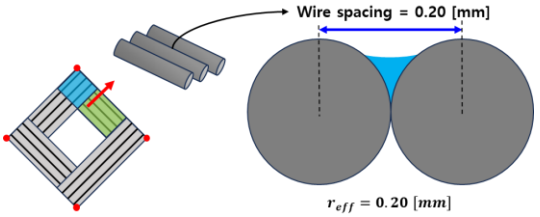

Fig. 6. Parallel wires model for the effective capillary radius of the braided wire wick.

Permeability

Permeability, K, is defined as the measure of the flow conductance of a porous medium based on Darcy's law and can be expressed in Eq. 9 [12]:

(9) $K = -\frac{\mu u_D}{dP/dx}$

μ is liquid viscosity, and dP/dx is pressure drop through the porous medium. u_D is filter velocity, which is related to the pore velocity u_p by $u_D = \varepsilon u_p$. The pore velocity is the local average velocity in the pore, and the filter velocity is the average velocity in the entire porous medium. The parallel wires can be considered the main capillary flow path in the same approach with the effective capillary radius. Therefore, as the models for the flow along the axis of the parallel wires, models by Happel and Brenner (1983) [13] and Gebart (1992) [14] were used as a base of the model in this work.

These models are based on the law of Hagen-Poiseuille, a base theory of the well-known Carman-Kozeny theory [15]. By assuming a fully developed laminar flow, the average pore velocity in a channel inside the wick can be obtained based on the Hagen-Poiseuille equation:

$$(10)\quad u_p = -\frac{2d_h^2}{c\mu}\frac{dP}{dx}$$

where d_h is the hydraulic diameter of the channel, and c is a shape factor of the channel. The permeability can be obtained as Eq. 11 by comparing Eq. 9 and Eq. 10 and using the relation between the filter and pore velocity.

$$(11)\quad K = \frac{2\varepsilon d_h^2}{c}$$

On the other hand, a unit cell of the capillary flow in the braided wire wick can be set as the cross-section of the flow between the wires, as shown in Fig. 7.

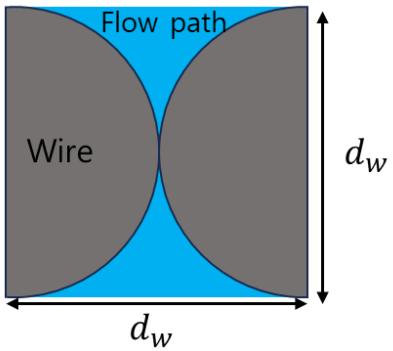

Fig. 7. A unit cell of the capillary flow in the braided wire wick.

Based on the unit cell, the hydraulic diameter of the flow in the braided wire wick, d_{h_B}, can be calculated as

$$(12)\quad d_{h\_B} = \frac{4A_l}{P_w} = \left(\frac{4}{\pi} - 1\right) d_w$$

where A_l is the liquid flow area, and P_w is the wetted perimeter. Furthermore, 53 was selected as a similar shape for the shape factor of an equilateral triangular cross-section [14].

Substitution of Eq. 12 and the shape factor in Eq. 11 yields the permeability of the braided wire wick, K_B:

$$(13)\quad K_B = \frac{2}{53}\left(\frac{4}{\pi} - 1\right)^2 \varepsilon_B d_w^2$$

By Eq. 13, the permeability of the braided wire wick in this work is 3.8×10^{-5} mm^2.

3. Measurements of capillary properties

A capillary rate-of-rise experiment [16] was conducted to validate the effective capillary radius and permeability evaluation results based on the models. The experiment requires visualizing the capillary flow through the braided wire wick. In this study, several preliminary experiments were conducted to confirm the feasibility of the visualization method and optimize it.

3.1. Capillary rise theory

The theory of the capillary rate-of-rise experiment is based on the capillary rise phenomenon. While liquid rising, the maximum capillary pressure, $\Delta P_{c,max}$ is balanced by viscous loss and hydrostatic pressure. Based on Darcy's law, the viscous loss in the porous medium can be evaluated, while the inertial effect can be neglected due to the low velocity. Thus, the governing equation of the liquid rise through the wick is given as Eq. 14 [16].

$$(14)\quad \Delta P_{c,max} = \frac{2\sigma}{r_{eff}} = \frac{\mu\varepsilon}{K}h(t)\frac{dh(t)}{dt} + \rho g h(t)$$

where σ, and ρ are the liquid's surface tension, and density, respectively. g is the gravitational acceleration, and h(t) is the height of the rise of the liquid with respect to time.

By solving Eq. 14 for the rise height, Eq. 15 is obtained as a solution as follows:

$$(15)\quad h(t) = A[1 + W(-\exp(-1 - Bt))]$$

$$(16)\quad A = \frac{2\sigma}{r_{eff}\rho g}$$

$$(17)\quad B = \frac{Kg^2\rho^2 r_{eff}}{2\sigma\mu\varepsilon}$$

where the function $W(x)$ is a Lambert W-function [17], and by a non-linear curve fitting the entire experimental data set with Eq. 15, the values of coefficients A and B in Eq. 16 and Eq. 17, respectively, can be obtained. The effective capillary radius and permeability can be obtained from those coefficients using the properties of the liquid. Additionally, it can be confirmed that the maximum capillary pressure is equal to the hydrostatic pressure at the steady state because, as time goes infinitely, the value of the Lambert W-function approaches zero.

3.2. Sample preparation

The braided wire wick proposed by KAERI was the sample for the experiment. The specifications of the sample are the same as in Table I. The wick was cut into 140 mm lengths. Fig. 8 shows side and cross-sectional views of the sample.

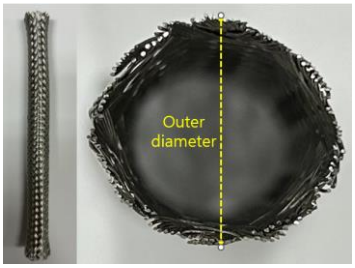

Fig. 8. Side and cross-sectional views of the wick sample.

After cutting, the samples were cleaned for 15 minutes using an ultrasonic cleaner with approximately 40℃ of Borer Chemie AG's deconex 11 UNIVERSAL alkalic cleaning solution. They were then cleaned again for 5 minutes in the ultrasonic cleaner with DI water and rinsed with DI water. Then, they were dried for 30 minutes in an oven at 40℃.

3.3. Experimental setup and measurement method

Fig. 9 schematically shows the experimental setup and methodology. The liquid for the experiment was 1 atm, 23.3°C DI water. As an infrared camera started to record, the braided wire wick sample was dipped 2 mm vertically into the DI water reservoir, and the rising liquid through the sample was recorded. The spatial and temporal resolution of the optical setup was 0.33 mm/pixel and 30 frames per second, respectively. The heights of the liquid's rise were measured with respect to time by visualizing the liquid interface. By fitting Eq. 15 to the measurements, the effective capillary radius and permeability can be obtained from the coefficients in Eq. 16 and Eq. 17.

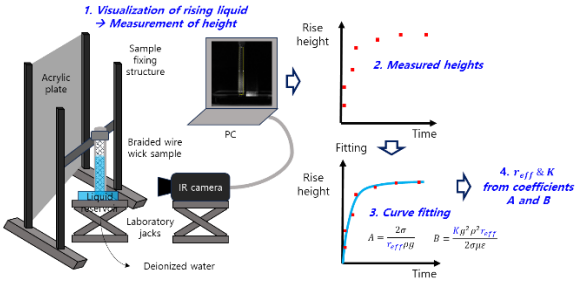

Fig. 9. Schematic of the experimental setup and methodology of the preliminary capillary rate-of-rise experiment.

As a method for visualization of the liquid interface, a high-speed camera (visible light) and another method using an infrared camera (infrared light) were conducted and compared. It was observed that there was about ten times larger signal noise in the technique using a high-speed camera. This seems to be because of the braided wire wick's high reflectivity and uneven surface. On the other hand, in the results of the method using an infrared camera, the inflection of the gray value distribution, which was caused by the emissivity difference between the wet and dry surfaces of the wick, was observed like the former research [18]. The visualization results of each method are in Fig. 10. Based on this, a visualization method using an infrared camera was selected.

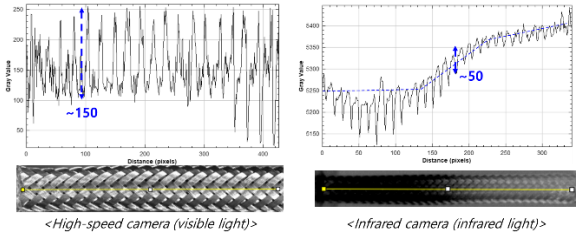

Fig. 10. Visualization results of the rising liquid's interface using a high-speed and infrared camera: Low noise.

The image processing sequence was conducted to enhance the detection capability of the liquid interface. As a first step, the pixel values in each horizontal line from the reference height of the wick region were averaged to reduce the noise. By averaging along the horizontal line, blurring of the liquid interface can be avoided. The noise was significantly reduced by using the average value as a representative value of the corresponding height. This noise reduction effect is shown in Fig. 11.

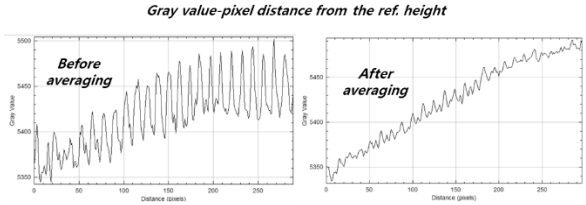

Fig. 11. Noise reduction effect of the averaging process of the pixel values in the wick along each horizontal line from the reference height.

After the averaging process, the difference between each raw image and the reference image, an image of a dry wick, was calculated to clearly classify wet and dry regions in the wick. Fig. 12 shows a schematic of this process and the result.

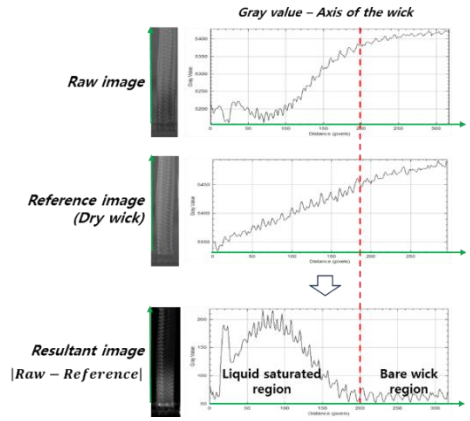

Fig. 12. Schematic of calculating the difference between raw and reference images (dry wick).

Fig. 13 depicts the final processed image, its region of interest, the averaging line of the pixel values, and the liquid rise height.

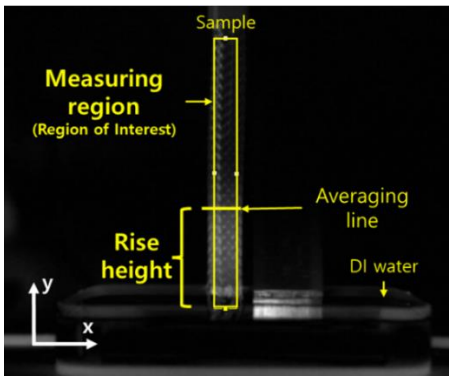

Fig. 13. Final processed image and its region of interest, averaging line of the pixel values and the liquid rise height.

The final image's gray value distribution allowed the detection of a liquid interface within certain uncertainties, depicted in Fig. 14 as 2δ, determined as one wavelength of a gray value fluctuation in the inflection region. The rise height was measured within the uncertainty $\pm\delta$ from the liquid surface, about 30 pixels away from the bottom of the region of interest. Fig. 14 shows a schematic of the liquid rise height measurement in the gray value distribution of the image.

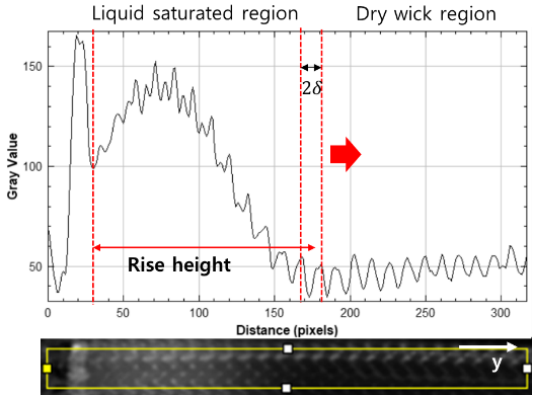

Fig. 14. Liquid rise height measurement from the gray value distribution in the processed image.

3.4. Results and discussions

Fig. 15 shows visualization data and the measurements of the rise heights from the experiments. Four samples were tested, and the average heights within standard deviations as uncertainties are depicted. The equation of the fitted curve is Eq. 18.

$$(18)\quad h_B(t) = 0.0673986[1 + W(-\exp(-1 - 0.0184t))]$$

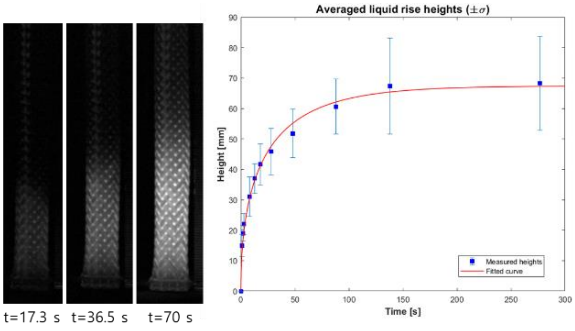

Fig. 15. Visualization data and the rise height data with a fitted curve of the capillary rate-or-rise experiment.

The coefficients of Eq. 18 were used to calculate the effective capillary radius and permeability. The porosity value calculated by Eq. 7 was used. The water's thermophysical properties were obtained from the National Institute of Standards and Technology (NIST) website. The experimental values of the capillary properties are listed in Table IV, along with the theoretical values from the models.

Table IV: Results of the capillary properties of the braided wire wick

Capillary property	Theoretical value	Experimental value
Porosity ε_B	0.21	-
Effective capillary radius r_{eff_B}	0.25 mm	0.219 mm
Permeability K_B	3.8×10^{-5} mm^2	2.9×10^{-5} mm^2

The theoretical values from the models were compared with the experimental values from the preliminary experiment. The effective capillary radius model predicted the experimental value within 14% of error. This seems to be because the pores in the area with two strands, the internal pore structures with smaller effective capillary radii than the open pores between the wires, were not considered. Regarding permeability, the model predicted the experimental value within about 27% of error. This overestimation could also be caused by not considering the internal pore structures.

4. Conclusion

In this study, theoretical models of the capillary properties, including porosity, effective capillary radius, and permeability of the braided wire wick, were established, and preliminary experiments were conducted to validate them. The models focused on the main capillary flow path of the braided wire wick, which was between the adjacent wires. For the porosity, a geometric model was established. The porosity was assessed by calculating the void and total wick volumes; the result was 0.21.

The effective capillary radius was theoretically evaluated using the wick structure model consisting of a

series of parallel wires, and the result was the wire spacing of 0.25 mm. The permeability was also theoretically evaluated using the model based on the law of Hagen-Poiseuille with the hydraulic diameter and shape factor of the cross-sectional area of the flow in the braided wire wick.

To validate the results of the theoretical evaluations of the effective capillary radius and permeability, the capillary rate-of-rise experiment can be conducted to measure the effective capillary radius and permeability experimentally. In this study, several preliminary capillary rate-of-rise experiments were conducted to confirm the feasibility of the visualization method and optimize it.

As tentative results from the experiments, the model of the effective capillary radius showed good agreement with the experimental data within about 14%. It seems the difference is because the pores in the area with two strands, the internal pore structures with smaller effective capillary radii than the open pores between the wires, were not considered. The model of the permeability somewhat overestimated the experimental value by 27%, and this seems also to be caused by not considering the internal pore structures. Therefore, it is thought that the internal pore structure in the area with two overlapped wire strands should be included in the models to enhance them. Furthermore, to apply the capillary property models in the heat pipe condition, the no-wire regions where the flow will occur in the actual heat pipe will ultimately need to be considered.

5. Future work

The models will be modified to consider the internal pore structure and no-wire regions. The detection criteria of the inflection point in the experiment will be established. Then, the repeated capillary rate-of-rise experiment will be conducted to confirm its replicability. Additionally, the same experiment using neutron radiography to detect the liquid interface will be conducted to validate the measurement method using infrared light by cross-checking each other.

Acknowledgment

This work was supported by the National Research Council of Science & Technology (NST) grant funded by the Korea government (MSIT). (No. CAP23061-100)

REFERENCES

[1] Byung Ha Park, Chan Soo Kim, Sung Hoon Choi and Sung Nam Lee, Key Technologies for Korean Space Heat Pipe Reactor, Nuclear Technology, pp. 1-11, 2024.
[2] Odhekar D. and Harris D. K., Experimental investigation of bendable heat pipes using sintered copper felt Wick., Thermal and Thermomechanical Proceedings 10th Intersociety Conference on Phenomena in Electronics Systems, 2006.
[3] Beard, D. et al., Sodium heat pipes for space and surface fission power., 15th International Energy Conversion Engineering Conference, 2017.
[4] Jiu Yu et al., Effect of the passage area ratio of wick on an ultra-thin vapour chamber with a spiral woven mesh wick, Applied Thermal Engineering, Vol. 196, 2021.
[5] Jiu Yu et al., Effect of spiral woven mesh liquid pumping action on the heat transfer performance of ultrathin vapour chamber, International Journal of Thermal Sciences, Vol. 182, 2022.
[6] Byung Ha Park and Chan Soo Kim, Parametric study of a high temperature heat pipe with hybrid wick structure, Transactions of the Korean Nuclear Society Virtual spring Meeting, 2021.
[7] Yong Tang et al., Experimental investigation of capillary force in a novel sintered copper mesh wick for ultra-thin heat pipes, Applied Thermal Engineering, Vol. 115, 2017.
[8] Huang Guangwen et al., Fabrication and capillary performance of a novel composite wick for ultra-thin heat pipes, International Journal of Heat and Mass Transfer, Vol. 176, 2021.
[9] Seok-Hwan Moon et al., Thermal Analysis and Testing of a Heat Pipe With Woven Wired Wick, IEEE Transactions on components, packaging, and manufacturing technology, Vol 4, No. 6, 2014.
[10] Jin Sung Lee and Chul Ju Kim, Analysis of Woven Wire Wick Structure for a Miniature Heat Pipe, Korean Journal of Air-Conditioning and Refrigeration Engineering, Vol. 13(1), pp. 18-24, 2001.
[11] Chi S. W., Heat Pipe Theory and Practice, New York: McGraw-Hill., pp. 35-38, 1976
[12] M. Kaviany, Principles of Heat Transfer in Porous Media, Springer New York, NY, 1995.
[13] J. Happel and H. Brenner, Low Reynolds number hydrodynamics, Martinus Nijhoff Publishers, 1983.
[14] B. R. Gebart, Permeability of Unidirectional Reinforcements for RTM, Journal of Composite Materials, Vol. 26, No. 8, 1992.
[15] F. A. L. Dullien, Single Phase Flow Through Porous Media and Pore Structure, The Chemical Engineering Journal, Vol. 10, pp. 1-34, 1975.
[16] Elkholy, A., Durfee, J., Mooney, J. P., Robinson, A. J., and Kempers, R., A rate-of-rise facility for measuring properties of Wick Structures. Measurement Science and Technology, 34(4), 045301, 2023.
[17] Barry, D. A., Parlange, J.-Y., Li, L., Prommer, H., Cunningham, C. J., and Stagnitti, F., Analytical approximations for real values of the Lambert w-function, Mathematics and Computers in Simulation, 53(1-2), 95-103, 2000
[18] Tang, Y., Deng, D., Lu, L., Pan, M. and Wang, Q., Experimental investigation on capillary force of composite wick structure by IR thermal imaging camera, Experimental Thermal and Fluid Science, Vol. 34, pp. 190-196, 2010.